Pulsatile Illumination for Photobiology and Optogenetics

Julia Dietler[1,‡], Robert Stabel[1,‡], and Andreas Möglich[1,2,3,4,*,‡]

[1]Lehrstuhl für Biochemie, [2]Research Center for Bio-Macromolecules, [3]Bayreuth Center for Biochemistry & Molecular Biology, [4]North-Bavarian NMR Center, Universität Bayreuth, Universität Bayreuth, 95447 Bayreuth, Germany.

[*]to whom correspondence may be addressed: andreas.moeglich@uni-bayreuth.de

[‡]ORCID identifiers: J.D. 0000-0002-0418-0796; R.S. 0000-0002-9159-0004; A.M. 0000-0002-7382-2772

Copyright Information

published as Dietler *et al.* (2019) *Meth Enzymol* **624**, 227-248.

http://dx.doi.org/doi:10.1016/bs.mie.2019.04.005

© 2019. This manuscript version is made available under the CC-BY-NC-ND 4.0 license https://creativecommons.org/licenses/by-nc-nd/4.0/

Running Title

Pulsatile Illumination for Photobiology and Optogenetics

Keywords

cyclic nucleotide; histidine kinase; light-oxygen-voltage; multiplexing; open electronics; optogenetics; photobiology; photocycle; phytochrome; sensory photoreceptor

Abstract

Living organisms exhibit a wide range of intrinsic adaptive responses to incident light. Likewise, in optogenetics, biological systems are tailored to initiate predetermined cellular processes upon light exposure. As genetically encoded, light-gated actuators, sensory photoreceptors are at the heart of these responses in both the natural and engineered scenarios. Upon light absorption, photoreceptors enter a series of generally rapid photochemical reactions leading to population of the light-adapted signaling state of the receptor. Notably, this state persists for a while before thermally reverting to the original dark-adapted resting state. As a corollary, the inactivation of

photosensitive biological circuits upon light withdrawal can exhibit substantial inertia. Intermittent illumination of suitable pulse frequency can hence maintain the photoreceptor in its light-adapted state while greatly reducing overall light dose, thereby mitigating adverse side effects. Moreover, several photoreceptor systems may be actuated sequentially with a single light color if they sufficiently differ in their inactivation kinetics. Here, we detail the construction of programmable illumination devices for the rapid and parallelized testing of biological responses to diverse lighting regimes. As the technology is based on open electronics and readily available, inexpensive components, it can be adopted by most laboratories at moderate expenditure. As we exemplify for two use cases, the programmable devices enable the facile interrogation of diverse illumination paradigms and their application in optogenetics and photobiology.

1. Introduction

Numerous organisms employ sensory photoreceptor proteins to derive spatial and temporal cues from incident light for the adjustment of physiology, behavior and lifestyle (Hegemann, 2008; Möglich et al., 2010). Photoreceptors double as genetically encoded, light-gated actuators in optogenetics (Deisseroth et al., 2006) to enable the non-invasive optical manipulation of diverse cellular processes with exquisite spatiotemporal resolution (Losi, Gardner, & Möglich, 2018). In the absence of light, sensory photoreceptors assume their thermodynamically most stable, dark-adapted state, denoted D in the following; absorption of light initiates a cyclic series of photochemical reactions, denoted photocycle, as part of which the light-adapted signaling state L is populated (Ziegler & Möglich, 2015). This photocycle is generally reversible, and the metastable state L persists for a while before passively, i.e. thermally, decaying to D in a process called dark recovery over the course of seconds to days, depending on photoreceptor. Based on the chromophore used for light absorption and the photochemistry exhibited, sensory photoreceptors divide into around ten families. As one family, light-oxygen-voltage (LOV) receptors bind flavin-nucleotide chromophores and respond to blue light (Christie et al., 1998; Salomon et al., 2001; Yee et al., 2015). Of note, the light-adapted state L of LOV receptors reverts to D in a strongly temperature-dependent, base-catalyzed reaction (Alexandre, Arents, van Grondelle, Hellingwerf, & Kennis, 2007), the kinetics of which can be deliberately varied over several orders of magnitude via modification of certain amino acids adjacent to the flavin chromophore (Pudasaini, El-Arab, & Zoltowski, 2015). Phytochromes (Phys) constitute a large receptor family sensitive to red and far-red light that occur in plants, (cyano)bacteria and fungi (Rockwell & Lagarias, 2010). In conventional

58 Phys, red light drives the transition of D to the light-adapted state L which returns to D either
59 thermally or through absorption of a second light quantum of far-red color.

60 Experiments in the neurosciences aside, optogenetic applications often take place on
61 comparatively long time scales and frequently involve the prolonged exposure to light of the system
62 under study. The underlying photoreceptors hence repeatedly transition between their dark-
63 adapted and light-adapted states D and L, and under constant illumination a photostationary state
64 is assumed. Rather than continuously illuminating throughout the experiment, light may also be
65 applied intermittently in pulsatile manner. By reducing the overall light dose (cf. below), this
66 approach can mitigate phototoxicity, photobleaching and sample heating. In addition, pulsed
67 illumination can enable the multiplexing of several light-sensitive systems and their selective
68 activation (Hennemann et al., 2018). We illustrate these aspects by means of two numerical
69 simulations (Fig. 1). In the first and conceptually simplest scenario, a given photoreceptor be
70 monomeric and assume either the D or L state. The forward transition D→L proceed with a
71 unimolecular rate constant k_1, dependent on the applied light intensity, and the backward reaction
72 L→D, i.e. the dark recovery, with a light-independent unimolecular rate constant k_{-1}. As shown in
73 Fig. 1B, during a train of light pulses the system repeatedly cycles between the D and L states as
74 determined by the relative magnitudes of the microscopic rate constants k_1 and k_{-1} and of the
75 applied pulse frequency. At least two points are of note: first, lighting schemes with the same overall
76 light dose may activate the photoreceptor to rather different average levels, depending upon the
77 timing of successive light pulses (left and right panels in Fig. 1B); second, two photoreceptor systems
78 may be discriminated in the pulse-frequency domain, albeit to limited extent, given the single-
79 exponential recovery kinetics. A second, more complex scenario considers a homodimeric
80 photoreceptor subjected to the same light-pulse sequence as before (Fig. 1C). For simplicity, we
81 assume that the two subunits of the receptor undergo the D↔L transition independently of
82 another with microscopic rate constants of k_1 and k_{-1}. As a consequence, the reaction from the fully
83 dark-adapted state DD to the fully light-adapted state LL, and *vice versa*, proceeds via the mixed-
84 state intermediates DL and LD, therefore giving rise to sigmoidal reaction kinetics instead of single-
85 exponential ones. For the present scope, we further assume that the receptor be cooperative
86 (Monod, Wyman, & Changeux, 1965) in that the LL, DL and LD states have the same output activity,
87 a situation that has been experimentally demonstrated for at least one photoreceptor system
88 (Möglich, Ayers, & Moffat, 2009). As illustrated in Fig. 1C, the homodimeric scenario also exhibits
89 higher average extents of light activation if a given light dose is spread over several shorter pulses
90 rather than concentrated in infrequent but longer pulses. In addition, the simulations show that the

91 sigmoidal reaction course enables a much better discrimination between two systems with different
92 recovery kinetics, thus allowing the sequential addressing of these systems by light of varying pulse
93 frequency and intensity (Hennemann et al., 2018). While, evidently, other and more complex
94 photoreceptor reaction schemes are conceivable, even the simple simulations compellingly show
95 that the response to light may drastically differ between systems. We note that during optogenetic
96 deployment, reaction steps downstream of photoreceptor activation, often nonlinear and
97 cooperative, may additionally contribute to complex recovery kinetics and response dynamics to
98 pulsatile light (Ziegler & Möglich, 2015).

99 To efficiently probe and subsequently exploit the response of optogenetic systems to
100 intermittently applied light, we built programmable arrays of light-emitting diodes (LEDs) that allow
101 the testing and application of multiple lighting regimes in parallel (Hennemann et al., 2018; Stüven
102 et al., 2019). Here, we recapitulate the construction of these arrays (section 2.) and their
103 deployment to two photoreceptor systems (sections 3. and 4.).

104 2. Programmable arrays of light-emitting diodes

105 2.1. Arrays with red/green/blue-emitting diodes

106 In this section, we detail the assembly of a programmable matrix of red/green/blue (RGB) three-
107 color LEDs based on an open-source Arduino microcontroller and commercially available electronics
108 (Hennemann et al., 2018). The setup allows the illumination from below of 64 wells of a standard
109 96-well microtiter plate (MTP) with programmable light signals of adjustable intensity, timing and
110 color (peak wavelengths of 470, 525 and 620 nm) (Figure 2). The wiring scheme (Fritzing file) of the
111 three-color LED setup can be obtained at http://www.moeglich.uni-bayreuth.de/en/software.

112 *Materials*

113 – Arduino Uno microcontroller (Arduino, Turin, Italy)
114 – Adafruit NeoPixel NeoMatrix 8x8 (Adafruit Industries, New York, USA)
115 – jumper wires (EXP GmbH, Saarbrücken, Germany)
116 – resistor 470 Ω (EXP GmbH)
117 – electrolytic capacitor 4700 µF, 10 V (EXP GmbH)
118 – breadboard (EXP GmbH)
119 – solder and soldering iron
120 – AC power supply 5 V, 4 A (EXP GmbH)

121 – *optional:* real-time clock DS3221 (Adafruit Industries)

122 *Protocol*

123 i. Optionally, a real-time clock (RTC) for enhanced temporal precision can be used. If so, place
124 the RTC on the breadboard and connect it to the 5 V power (5V) and ground (GND) pins of the
125 Arduino board using jumper wires. Further, connect the SCL (serial clock line) and SDA (serial
126 data line) pins of the RTC to the analog inputs 4 and 5, respectively, of the Arduino board.
127 ii. Connect the 5V and GND pins of the Arduino board to the '+' and '-' rows of the breadboard.
128 Now, any pin/wire inserted into these rows will also be connected to power or ground,
129 respectively.
130 iii. Connect the electrolytic capacitor by attaching its cathode (short leg) to the '-' row and its
131 anode (long leg) to the '+' row of the board.
132 iv. Place the 470 Ω resistor on the breadboard and connect it to the digital pin 6 of the Arduino
133 microcontroller.
134 v. Connect the 5V and GND pins of the NeoPixel LED matrix to '+'/'-' on the breadboard; connect
135 the DIN pin to the resistor. To secure the connections, the jumper wires can be soldered in
136 place.

137 ## 2.2. Arrays with custom light-emitting diodes

138 Here, we describe a dual-color array that uses custom LEDs (Stüven et al., 2019). The setup allows
139 the illumination from below of 64 wells of a standard 96-well MTP with programmable light signals
140 of adjustable intensity, timing and two custom colors. In the example detailed here, LEDs with peak
141 wavelengths of 655 and 850 nm are used, but the design also applies to other LEDs of diverse colors.

142 *Materials*

143 – Arduino Uno microcontroller (Arduino)
144 – ITEAD Full Color RGB LED Matrix Driver Shield (Itead, Shenzhen, China)
145 – jumper wires (EXP GmbH)
146 – resistor 470 Ω (EXP GmbH)
147 – electrolytic capacitor 4700 µF, 10 V (EXP GmbH)
148 – breadboard (EXP GmbH)
149 – solder and soldering iron
150 – AC power supply 5 V, 4 A (EXP GmbH)

151 – 64x 3-mm LED color #1 [e.g., Kingbright WP908A8SRD, (655 ± 20) nm, Mouser Electronics,
152 Munich, Germany]
153 – 64x 3-mm LED color #2 [e.g., Harvatek HE1-120AC-XXXX (850 ± 42) nm, Conrad Electronic SE,
154 Hirschau, Germany]
155 – printed circuit board (PCB) [Eagle template file (.brd) and wiring scheme (.sch) are available at
156 http://www.moeglich.uni-bayreuth.de/en/software]
157 – *optional:* real-time clock DS3221 (Adafruit Industries)

158 *Protocol*

159 i. Print the custom circuit board according to the Eagle template file (.brd). Electronics shops or
160 dedicated companies, such as PCBAStore (http://www.pcbastore.com), EasyEDA
161 (http://easyeda.com), Pad2pad (http://www.pad2pad.com), or ExpressPCB
162 (http://www.expresspcb.com), can routinely do this for a small fee.
163 ii. Position the two sets of 64 LEDs on the PCB according to the wiring scheme (.sch) and solder
164 them in place.
165 iii. Connect the LED driver shield to the Arduino microcontroller such that the pins on both
166 elements line up.
167 iv. Use jumper wires to connect the assembled PCB and the LED driver shield according to the
168 wiring scheme.

169 ## 2.3. Housing and adapters for the LED arrays

170 The above LED arrays need to be embedded in a custom-made mounting adapter that reduces
171 light contamination between adjacent LEDs and allows positioning of an MTP on top such that it can
172 be illuminated from below. As one option, the required adapter pieces may be obtained by
173 subtractive manufacturing, which is offered by various companies. As described below, alternatively
174 the pieces can be obtained by 3D printing.

175 *Materials*

176 – template files for the base plate and mounting adapter (.stl files available at
177 http://www.moeglich.uni-bayreuth.de/en/software)
178 – 3D printer, e.g., Anycubic I3 MEGA (GearBest, China)
179 – polylactic acid (PLA) print filament, ideally in black (available from diverse suppliers)

180 *Protocol*

181 i. There are separate versions of the adapter pieces for the RGB (cf. 2.1.) and the custom LED
182 arrays (cf. 2.2.); ensure to use the correct one. Prior to printing, the template file for the
183 adapter pieces can be further adjusted to accommodate individual needs (e.g., different
184 MTPs, incubator platforms etc.). To this end, free software for computer-aided design, e.g.,
185 TinkerCAD (http://www.tinkercad.com), can be used.

186 ii. Print bottom and top piece of the adapter using PLA filament, a fill factor between 25 and
187 50%, and a precision of 100 µm. Use of ABS filament is not recommended as it is prone to
188 warping. We found that the print precision of consumer-grade printers is fully sufficient for
189 the task. Alternatively, printing can be done by 3D-printing services, such as Proto Labs
190 (http://www.protolabs.com), i.materialise (http://all3dp.com) or 3D Hubs
191 (http://www.3dhubs.com).

192 iii. Remove residual filament from the printed pieces using pliers and scissors.

193 iv. Place LED array on bottom adapter piece, then cover with top piece.

194 ## 2.4. Configuration and calibration of the LED arrays

195 To facilitate the configuration of the programmable LED matrices, we supply a Python-based
196 graphical user interface (GUI). As output, the interface generates an Arduino sketch file (.ino) that
197 needs to be compiled and uploaded to the Arduino board. Optionally, a light power meter may be
198 used to calibrate the intensity of the programmable LED arrays.

199 *Materials*

200 – USB-A to USB-B cable

201 – Python-based LED controller interface (available at http://www.moeglich.uni-
202 bayreuth.de/en/software)

203 – Arduino Integrated Development Environment (IDE) (available at http://www.arduino.cc)

204 – *optional:* light power meter (model 842-PE, Newport, Darmstadt, Germany)

205 – *optional:* silicon photodetector (model 918D-UV-OD3, Newport)

206 *Protocol*

207 i. Identify the version of the GUI applicable to the LED matrix you are using (RGB, cf. 2.1.; or
208 custom LEDs, cf. 2.2.) and download the corresponding Python file. The program can be
209 executed with Python version 3 on Windows, Linux and OS X platforms. Alternatively, for
210 Windows platforms, we supply a stand-alone binary file.

211 ii. Use the GUI to configure the timing scheme and brightness of each LED individually. Note that
212 the brightness of the LEDs is set by pulse-width modulation (PWM) on an 8-bit scale.
213 iii. *optional*: To enhance the temporal accuracy of the Arduino board (which can be quite
214 modest), an RTC module (cf. above) may be included. If so, a checkbox in the GUI should be
215 activated.
216 iv. Once the configuration is completed, the current settings can be saved as a configuration file
217 (.cfg). Export the configuration as an Arduino sketch file (.ino), close the GUI.
218 v. Start the Arduino IDE and open the (.ino) file generated in the previous step. At first use,
219 Arduino driver libraries for the RTC and, in case of the RGB LED matrix (cf. 2.1.), the NeoPixel
220 matrix need to be installed. To this end, select 'Manage Libraries' from the 'Sketch→Include
221 Library' pull-down menu. Locate the 'RTClib' and 'Adafruit NeoMatrix' entries and install the
222 libraries as required.
223 vi. Advanced users may optionally wish to directly modify the Arduino sketch file rather than use
224 the GUI. Connect the Arduino board to the computer via the USB cable, compile the program
225 code and upload it to the board.
226 vii. Provided no errors occurred, the LED array should now start lighting up as configured.
227 viii. *optional*: The actual light output of the LED matrix for given intensity settings may be
228 calibrated with a lamp power meter. To this end, place the detector of the lamp power meter
229 directly atop the upper piece of the LED assembly and measure the emitted light output for
230 several software intensity settings. Owing to the use of PWM, we found the set and actual
231 light intensities to be linearly correlated. Variations between different LEDs of the matrix were
232 found to be negligible. Note that the light output may depend on the power supply attached
233 to the LED matrix; hence, the calibration should be done for the power supply to be used in
234 the actual experiment.

235 3. Control of bacterial gene expression by varying light intensity and pulse frequency

236 We deployed the programmable RGB LED matrix (cf. 2.1.) to systematically chart the response of
237 the YF1/*Bj*FixJ two-component system (TCS) (Hennemann et al., 2018), as implemented on the
238 pDusk plasmid (Ohlendorf et al., 2012), to intermittently applied blue light of varying intensity (Fig.
239 3A). Briefly, the LOV receptor YF1 derives from the fusion of the photosensor module of *Bacillus*
240 *subtilis* YtvA and the effector module of the *Bradyrhizobium japonicum Bj*FixL histidine kinase
241 (Möglich et al., 2009). Provided both LOV sensors of the homodimeric YF1 reside in their dark-
242 adapted states (denoted DD), the receptor readily phosphorylates the so-called response regulator

243 (RR) *Bj*FixJ. In its phosphorylated form, the RR drives the expression from cognate promoters, e.g.,
244 of the red-fluorescent reporter *Ds*Red (Strack et al., 2008). Upon blue-light absorption by the LOV
245 modules, YF1 assumes the photochemically mixed states DL and LD or the fully light-adapted state
246 LL, all of which act as a phosphatase on phospho-*Bj*FixJ (Möglich et al., 2009). As for other LOV
247 receptors, the light-adapted state thermally returns to the dark-adapted state in the dark recovery
248 reaction. Certain residue exchanges placed near the flavin chromophore of the LOV sensor can
249 strongly modulate the kinetics of dark recovery (Pudasaini et al., 2015). Specifically, within the
250 pDusk context, we replaced valine 28 of YF1 by isoleucine which resulted in greatly decelerated
251 recovery kinetics (Hennemann et al., 2018; Kawano et al., 2013). As explained in the below protocol,
252 we assessed the impact of different blue-light regimes on *Ds*Red reporter expression from pDusk
253 plasmids encoding the original YF1 receptor or its V28I variant.

254 *Materials*

255 – plasmid pDusk encoding a fluorescent reporter such as *Ds*Red (plasmid pDusk available from
256 Addgene, plasmid 43795)
257 – *Escherichia coli* expression strain, e.g., BL21 or CmpX13 (Mathes et al., 2009)
258 – lysogeny broth medium supplemented with 50 µg mL^{-1} kanamycin (LB/Kan)
259 – programmable RGB LED matrix (cf. 2.1. and 2.3.)
260 – black-wall clear-bottom 96-well MTPs (Greiner BioOne, Frickenhausen, Germany)
261 – black 96-well MTPs (e.g., Greiner)
262 – transparent 96-well MTPs (e.g., Greiner)
263 – gas-permeable sealing film (BF-410 400-S, Corning, New York, USA)
264 – incubator, e.g., HN-2 Herp Nursery II (Lucky Reptile, Waldkirch, Germany)
265 – MTP shaker, e.g., PMS-1000i (Grant Instruments, Cambridge, UK)
266 – multimode MTP reader, e.g., Tecan Infinite M200 PRO (Tecan Group Ltd., Männedorf,
267 Switzerland)

268 *Protocol*

269 i. Transform between 10 pg and 100 ng of the pDusk-*Ds*Red plasmid into *E. coli* CmpX13 cells,
270 plate on LB/Kan agar and incubate over night at 37 °C. (Note that here and in the following
271 experimental steps, we assume that the *Ds*Red reporter and *E. coli* CmpX13 cells are used.
272 However, other fluorescent proteins and *E. coli* BL21 strains may be used instead.)
273 ii. Inoculate a 5-mL LB /Kan starter culture with a single clone from a freshly transformed plate
274 and incubate at 37 °C until an optical density at 600 nm (OD_{600}) of 0.3 is reached.

275 iii. Take 10 µL of the starter culture and inoculate 15 mL of pre-warmed LB/Kan medium.
276 iv. Mix thoroughly and dispense 200 µL each to 64 wells (use rows A-H and columns 1-8) of a
277 black-wall, clear-bottom 96-well MTP using a multichannel pipette.
278 v. Seal the MTP with a gas-permeable film to allow sufficient air circulation during subsequent
279 incubation.
280 vi. Configure the LED matrix according to chapter 2. For the study of light-dependent gene
281 expression in pDusk, we varied the intensity of blue light (470 nm) between 0 and 130 $\mu W\ cm^{-2}$
282 and used a periodic illumination scheme where individual wells were exposed to light for 30
283 s before incubation in the dark for periods between 0 and 65 min. The alternating dark/light
284 cycles continued until the end of the incubation (Hennemann et al., 2018).
285 vii. Place the sealed MTP plate on top of the configured LED-array setup. If necessary, fix the plate
286 in position with duct tape.
287 viii. Mount the assembly on an MTP shaker, place inside a suitable incubator and incubate at 37 °C
288 and 600 rpm for 16 h. Continuous shaking throughout the entire experiment promotes
289 aeration of the cultures and ensures their homogenous mixing and illumination. Ensure that
290 the incubator is tightly sealed against stray light from the outside and stays closed for the
291 entire experiment.
292 ix. Remove the sealing film. Using a multi-channel pipette, transfer 40 µL of each culture to a
293 transparent MTP and add 210 µL H_2O. Measure OD_{600} of each well in an MTP reader. If
294 absorbance falls outside the interval 0.1 - 1.0, prepare another solution of the bacterial
295 cultures at an appropriate dilution factor.
296 x. Using a multi-channel pipette, transfer 40 µL of the diluted solutions from the previous step
297 to a black MTP and add 210 µL H_2O. Measure reporter fluorescence of each well in an MTP
298 reader. To monitor *Ds*Red fluorescence, we used excitation and emission wavelengths of (554
299 ± 9) and (591 ± 20) nm, respectively. For optimal results, adjust the gain and focal height of
300 the MTP reader. To allow comparison between experiments on different days, these settings
301 must be left unchanged.
302 xi. Normalize fluorescence data to OD_{600} and plot as 2D contours plots as a function of the
303 duration of the dark period and the intensity of pulsed illumination (Fig. 3B).
304 xii. As the expected result, the *Ds*Red reporter-gene output for either YF1 or V28I should decrease
305 monotonically with light intensity (ordinate in Fig. 3B) but increase monotonically with the
306 length of the dark period (abscissa). In comparison to the original YF1, the V28I variant with

307 slower dark-recovery kinetics is toggled by lower overall light doses, i.e. it is more light-
308 sensitive.

309 ## 4. Engineering and characterization of photoactivated adenylyl cyclases

310 We originally developed the programmable arrays with custom LEDs (cf. 2.2.) to probe the
311 response of certain photoactivated adenylyl cyclases (PAC) to red/far-red light regimes of varying
312 intensity and timing (Stüven et al., 2019). Briefly, PACs mediate the production of the versatile
313 second messenger 3', 5' cyclic adenosine monophosphate (cAMP) in a light-stimulated manner.
314 Several naturally occurring, mostly blue-light-sensitive PACs (Blain-Hartung et al., 2018; Iseki et al.,
315 2002; Raffelberg et al., 2013; Ryu, Moskvin, Siltberg-Liberles, & Gomelsky, 2010; Schröder-Lang et
316 al., 2007; Stierl et al., 2011) have been supplemented by engineered PACs that respond to red and
317 far-red light (Etzl et al., 2018; Ryu et al., 2014; Stüven et al., 2019). These PACs are based on
318 bacteriophytochrome (BPhy) sensor units and can be bidirectionally toggled between two functional
319 states by red and far-red light, respectively, thus potentially enhancing the precision in time and
320 space of optogenetic applications (Ziegler & Möglich, 2015). Moreover, red and far-red light exhibit
321 deeper penetration of biological tissue than blue light (Weissleder, 2001), thus rendering BPhy-
322 based PACs attractive for optogenetics *in vivo*. To rapidly assess the light-dependent activity of PACs,
323 we established the pCyclR reporter-gene assay in *E. coli*, as illustrated in Fig. 4A (Stüven et al., 2019).
324 In this assay, the functional expression of PACs, followed by stimulation with light of suitable quality
325 and quantity, prompts the intracellular production of cAMP. In turn, the endogenous *E. coli*
326 catabolite activator protein binds cAMP and activates the expression of the red-fluorescent reporter
327 *Ds*Red. By resorting to this assay, we engineered the photoreceptor *Dd*PAC which displays cAMP
328 production that is elevated and diminished by exposure to red and far-red light, respectively. The
329 two protocols below illustrate the application of the pCyclR reporter system to record the response
330 of *Dd*PAC to red and far-red light of varying intensity (protocol A, Fig. 4B) and timing (protocol B,
331 Fig. 4C).

332 ### *Materials*

333 – pCyclR reporter plasmid (kanamycin resistance marker; available from the authors)
334 – pCDF plasmid harboring expression cassettes for *Dd*PAC and *Synechocystis* sp. heme
335 oxygenase (streptomycin resistance marker; available from the authors)
336 – adenylyl-cyclase-deficient *E. coli* strain CmpX13 Δ*cyaA* (available from the authors)

337 – lysogeny broth medium supplemented with 50 µg mL^{-1} kanamycin and 100 µg mL^{-1}
338 streptomycin (LB/Kan+Strep)
339 – isopropyl β-D-1-thiogalactopyranoside (IPTG; 1 M stock solution)
340 – programmable matrix with 655-nm and 850-nm LEDs (cf. 2.2. and 2.3.)
341 – black-wall clear-bottom 96-well MTPs (Greiner)
342 – black 96-well MTPs (e.g., Greiner)
343 – transparent 96-well MTPs (e.g., Greiner)
344 – gas-permeable sealing film (BF-410 400-S, Corning)
345 – incubator, e.g., HN-2 Herp Nursery II (Lucky Reptile)
346 – MTP shaker, e.g., PMS-1000i (Grant Instruments)
347 – multimode MTP reader, e.g., Tecan Infinite M200 PRO (Tecan Group Ltd.)

348 *Protocol A*

349 i. Transform between 10 pg and 100 ng each of the pCyclR reporter and the pCDF expression
350 plasmids into *E. coli* CmpX13 *ΔcyaA* cells, plate on LB/Kan+Strep agar and incubate over night
351 at 37 °C. If efficiency is insufficient, transform the two plasmids sequentially. (Note that here
352 and in the following experimental steps, we assume that the pCDF *Dd*PAC expression plasmid
353 and *E. coli* CmpX13 *ΔcyaA* cells are used. However, other PAC proteins and cyclase-deficient
354 *E. coli* BL21 strains may be used instead.)
355 ii. Inoculate a 5-mL LB/Kan+Strep starter culture with a single clone from a freshly transformed
356 plate and incubate over night at 37 °C.
357 iii. Dispense 180 µL LB/Kan+Strep each to 64 wells (use rows A-H and columns 1-8) of a black-
358 wall, clear-bottom 96-well MTP using a multichannel pipette. Inoculate each well with 2 µL of
359 the over-night culture.
360 iv. Seal the MTP with a gas-permeable film to allow sufficient air circulation during subsequent
361 incubation.
362 v. Place the MTP on a shaker and incubate at 37 °C and 800 rpm for 1 h in darkness.
363 vi. Add 60 µL of 0.2 mM IPTG in LB/Kan+Strep to each well. The resultant final IPTG concentration
364 of 50 µM proved ideal for *Dd*PAC; however, other PACs may require different inductor
365 concentrations.
366 vii. Configure the LED matrix according to chapter 2. For the study of *Dd*PAC activation by constant
367 illumination, we varied the intensity of red (peak emission 655 nm) and far-red light (850 nm)
368 between 0 and 80 µW cm^{-2} (Stüven et al., 2019).

369 viii. Place the sealed MTP plate on top of the configured LED-array setup. If necessary, fix the plate
370 in position with duct tape.
371 ix. Mount the assembly on an MTP shaker, place inside a suitable incubator and incubate at 37 °C
372 and 800 rpm for 22 h. Ensure that the incubator is tightly sealed against stray light from the
373 outside and stays closed for the entire experiment.
374 x. Remove the sealing film. Using a multi-channel pipette, transfer 25 µL of each culture to a
375 transparent MTP and add 225 µL H_2O. Measure OD_{600} of each well in an MTP reader. If
376 absorbance falls outside the interval 0.1 - 1.0, prepare another solution of the bacterial
377 cultures at an appropriate dilution factor.
378 xi. Using a multi-channel pipette, transfer 50 µL of the diluted solutions from the previous step
379 to a black MTP and add 200 µL H_2O. Measure reporter fluorescence of each well in an MTP
380 reader. To monitor *Ds*Red fluorescence, we used excitation and emission wavelengths of (554
381 ± 9) and (591 ± 20) nm, respectively. For optimal results, adjust the gain and focal height of
382 the MTP reader. To allow comparison between experiments on different days, these settings
383 must be left unchanged.
384 xii. Normalize fluorescence data to OD_{600} and plot as a function of the intensity of red/far-red
385 illumination, e.g., using the open-source Fit-o-mat software (Möglich, 2018) (Fig. 4B).
386 xiii. As the expected result, the *Ds*Red reporter-gene output should increase hyperbolically with
387 red-light intensity but should stay constant at a basal level for far-red illumination.

388 *Protocol B*

389 i. Follow steps i.-vi. as described for protocol A.
390 ii. Configure the LED matrix according to chapter 2. For the study of *Dd*PAC activation by pulsed
391 illumination, we used a red-light (peak emission 655 nm) intensity of 40 µW cm^{-2}. In periodic
392 manner, illumination for 60 s was followed by incubation in darkness for between 0 and 3,600
393 s. The alternating dark/light cycles continued until the end of the incubation (Stüven et al.,
394 2019).
395 iii. Follow steps viii.-xii. as described for protocol A.
396 iv. As the expected result, the *Ds*Red reporter-gene output should increase hyperbolically with
397 the duty cycle of red-light exposure (Fig. 4C), where the duty cycle denotes the fraction of
398 time during which light was applied.

399 5. Summary and conclusion

400 Beyond variation of light quantity (intensity) and quality (color), the timing of intermittently
401 applied light affords an additional input dial for adjusting the output of optogenetic systems.
402 Pulsatile illumination offers at least two principal advantages (Hennemann et al., 2018): first,
403 carefully chosen lighting sequences can significantly lower the required overall light dose, thus
404 reducing phototoxicity, photobleaching and heat input, but retaining the desired optogenetic
405 output. Second, intermittent light facilitates the parallel deployment of several light-regulated
406 circuits even when they are sensitive to the same light quality (i.e. wavelength), as long as they differ
407 in their response to pulsatile light. As exemplified for the pDusk variants YF1 and V28I (cf. 3.), a
408 single light color suffices for successively actuating two systems, thus freeing up optical input
409 channels that may be used for other optogenetic actuators and fluorescent reporters. The exact
410 response to pulsed illumination is primarily governed by the reversal kinetics of the system in
411 question, i.e. how fast is the dark-adapted state regained after prior light exposure, but other
412 aspects matter as well. Whereas in simple scenarios these kinetics are of single-exponential form
413 (cf. Fig. 1B), the output of other systems may be governed by oligomeric species and cooperative
414 effects, thus giving rise to non-exponential and more complex reversal kinetics (cf. Fig. 1C). This type
415 of cooperativity has indeed been observed for certain homodimeric photoreceptors (Möglich et al.,
416 2009) and is generally expected to at least some extent for light-mediated reactions that involve
417 two or more light-responsive entities. As a case in point, the plant cryptochrome 2 is known to
418 undergo light-dependent homo-oligomerization which has been amply exploited for optogenetic
419 intervention in different cellular processes (Bugaj et al., 2015; Bugaj et al., 2013; Losi et al., 2018;
420 Taslimi et al., 2014). Moreover, reaction sequences downstream of the photoreceptor and en route
421 to the eventual optogenetic output may entail nonlinear and thresholding effects, thus further
422 altering the response dynamics of the system to (pulsed) illumination. Taken together, the relevant
423 response kinetics may be challenging to gauge upfront and should ideally be assessed on a case-by-
424 case basis for each optogenetic system.

425 Against this backdrop, the advent of affordable, customizable, parallelizable and programmable
426 illumination devices appears particularly relevant. Numerous light intensities and timing schemes
427 can be interrogated in parallel and facile manner, thus allowing the response characteristics of a
428 given light-sensitive system to be precisely mapped. Provided two such systems sufficiently differ in
429 that regard, they can be sequentially activated by a single light color (cf. Fig. 3 and (Hennemann et
430 al., 2018)). To fully capitalize on the enhanced throughput for light-mediated actuation, the
431 recording of the system response should support commensurate throughput. On the one hand,
432 reporter-gene assays, as demonstrated here (cf. 3. and 4.), apply as they efficiently report on the

433 activity of the light-responsible system, even if only in indirect manner. On the other hand, one may
434 directly monitor the desired optogenetic response of the system under study if it gives rise to a
435 readily recordable phenotype.

436 The programmable arrays of light-emitting diodes used here are entirely based on open
437 electronics and commercially available parts. Hence, most laboratories will be able to assemble
438 them at moderate expenditure of time and cost. Our setups (Hennemann et al., 2018; Stüven et al.,
439 2019) and a host of related ones for programmable illumination (Chen et al., 2012; Davidson, Basu,
440 & Bayer, 2013; Gerhardt et al., 2016; Heo et al., 2015; Lee et al., 2014; Pilizota & Yang, 2018; Richter
441 et al., 2015; Szymula et al., 2018) now allow the routine testing of multiple lighting settings and
442 efficient exploration of the accessible parameter space. As discussed above, this methodology
443 particularly benefits optogenetics but it also extends to other light-dependent biological and even
444 chemical phenomena, with pertinent examples being the growth dynamics of photoautotrophic
445 organisms (Reimers et al., 2017), the activity of light-driven enzymes (Sorigué et al., 2017), and the
446 photocatalysis of diverse chemical conversions (König, 2013; Romero & Nicewicz, 2016).

447 Acknowledgements

448 We thank our colleagues in the Möglich laboratory for discussion; Dr. Markus Lippitz for advice
449 on the design of the programmable LED arrays; and the electronics shop at the University of
450 Bayreuth for help with the assembly. This work was supported by grant MO2192/4-1 (to A.M.) by
451 the Deutsche Forschungsgemeinschaft.

452 References

453 Alexandre, M. T. A., Arents, J. C., van Grondelle, R., Hellingwerf, K. J., & Kennis, J. T. M. (2007). A
454 Base-Catalyzed Mechanism for Dark State Recovery in the Avena sativa Phototropin-1 LOV2
455 Domain. *Biochemistry*, *46*(11), 3129–3137. https://doi.org/10.1021/bi062074e
456 Blain-Hartung, M., Rockwell, N. C., Moreno, M. V., Martin, S. S., Gan, F., Bryant, D. A., & Lagarias, J.
457 C. (2018). Cyanobacteriochrome-based photoswitchable adenylyl cyclases (cPACs) for broad
458 spectrum light regulation of cAMP levels in cells. *Journal of Biological Chemistry*, *293*(22),
459 8473–8483. https://doi.org/10.1074/jbc.RA118.002258
460 Bugaj, Lukasz J., Choksi, A. T., Mesuda, C. K., Kane, R. S., & Schaffer, D. V. (2013). Optogenetic protein
461 clustering and signaling activation in mammalian cells. *Nature Methods*, *10*(3), 249–252.
462 https://doi.org/10.1038/nmeth.2360

463 Bugaj, L. J., Spelke, D. P., Mesuda, C. K., Varedi, M., Kane, R. S., & Schaffer, D. V. (2015). Regulation
464 of endogenous transmembrane receptors through optogenetic Cry2 clustering. *Nature*
465 *Communications*, *6*, 6898. https://doi.org/10.1038/ncomms7898
466 Chen, M., Mertiri, T., Holland, T., & Basu, A. S. (2012). Optical microplates for high-throughput
467 screening of photosynthesis in lipid-producing algae. *Lab on a Chip*, *12*(20), 3870–3874.
468 https://doi.org/10.1039/c2lc40478h
469 Christie, J. M., Reymond, P., Powell, G. K., Bernasconi, P., Raibekas, A. A., Liscum, E., & Briggs, W. R.
470 (1998). Arabidopsis NPH1: a flavoprotein with the properties of a photoreceptor for
471 phototropism. *Science*, *282*(5394), 1698–1701.
472 Davidson, E. A., Basu, A. S., & Bayer, T. S. (2013). Programming microbes using pulse width
473 modulation of optical signals. *Journal of Molecular Biology*, *425*(22), 4161–4166.
474 https://doi.org/10.1016/j.jmb.2013.07.036
475 Deisseroth, K., Feng, G., Majewska, A. K., Miesenböck, G., Ting, A., & Schnitzer, M. J. (2006). Next-
476 generation optical technologies for illuminating genetically targeted brain circuits. *Journal of*
477 *Neuroscience*, *26*(41), 10380–10386. https://doi.org/10.1523/JNEUROSCI.3863-06.2006
478 Etzl, S., Lindner, R., Nelson, M. D., & Winkler, A. (2018). Structure-guided design and functional
479 characterization of an artificial red light–regulated guanylate/adenylate cyclase for
480 optogenetic applications. *Journal of Biological Chemistry*, *293*(23), 9078–9089.
481 https://doi.org/10.1074/jbc.RA118.003069
482 Gerhardt, K. P., Olson, E. J., Castillo-Hair, S. M., Hartsough, L. A., Landry, B. P., Ekness, F., … Tabor, J.
483 J. (2016). An open-hardware platform for optogenetics and photobiology. *Scientific Reports*,
484 *6*, 35363. https://doi.org/10.1038/srep35363
485 Hegemann, P. (2008). Algal sensory photoreceptors. *Annual Review of Plant Biology*, *59*, 167–189.
486 https://doi.org/10.1146/annurev.arplant.59.032607.092847
487 Hennemann, J., Iwasaki, R. S., Grund, T. N., Diensthuber, R. P., Richter, F., & Möglich, A. (2018).
488 Optogenetic Control by Pulsed Illumination. *Chembiochem*, *19*(12), 1296–1304.
489 https://doi.org/10.1002/cbic.201800030
490 Heo, J., Cho, D.-H., Ramanan, R., Oh, H.-M., & Kim, H.-S. (2015). PhotoBiobox: A tablet sized, low-
491 cost, high throughput photobioreactor for microalgal screening and culture optimization for
492 growth, lipid content and CO2 sequestration. *Biochemical Engineering Journal*, *103*, 193–
493 197. https://doi.org/10.1016/j.bej.2015.07.013

494 Iseki, M., Matsunaga, S., Murakami, A., Ohno, K., Shiga, K., Yoshida, K., … Watanabe, M. (2002). A
495 blue-light-activated adenylyl cyclase mediates photoavoidance in *Euglena gracilis*. *Nature*,
496 *415*(6875), 1047–1051. https://doi.org/10.1038/4151047a
497 Kawano, F., Aono, Y., Suzuki, H., & Sato, M. (2013). Fluorescence Imaging-Based High-Throughput
498 Screening of Fast- and Slow-Cycling LOV Proteins. *PLoS ONE*, *8*(12), e82693.
499 https://doi.org/10.1371/journal.pone.0082693
500 König, B. (2013). *Chemical Photocatalysis*. Berlin, Boston: De Gruyter.
501 https://doi.org/10.1515/9783110269246
502 Lee, J. M., Lee, J., Kim, T., & Lee, S. K. (2013). Switchable gene expression in Escherichia coli using a
503 miniaturized photobioreactor. *PloS One*, *8*(1), e52382.
504 https://doi.org/10.1371/journal.pone.0052382
505 Losi, A., Gardner, K. H., & Möglich, A. (2018). Blue-Light Receptors for Optogenetics. *Chemical*
506 *Reviews*, *118*(21), 10659–10709. https://doi.org/10.1021/acs.chemrev.8b00163
507 Mathes, T., Vogl, C., Stolz, J., & Hegemann, P. (2009). In vivo generation of flavoproteins with
508 modified cofactors. *Journal of Molecular Biology*, *385*(5), 1511–1518.
509 https://doi.org/10.1016/j.jmb.2008.11.001
510 Möglich, A. (2018). An Open-Source, Cross-Platform Resource for Nonlinear Least-Squares Curve
511 Fitting. *Journal of Chemical Education*, *95*(12), 2273–2278.
512 https://doi.org/10.1021/acs.jchemed.8b00649
513 Möglich, A., Ayers, R. A., & Moffat, K. (2009). Design and signaling mechanism of light-regulated
514 histidine kinases. *Journal of Molecular Biology*, *385*(5), 1433–1444.
515 https://doi.org/10.1016/j.jmb.2008.12.017
516 Möglich, A., Yang, X., Ayers, R. A., & Moffat, K. (2010). Structure and function of plant
517 photoreceptors. *Annual Review of Plant Biology*, *61*, 21–47.
518 https://doi.org/10.1146/annurev-arplant-042809-112259
519 Monod, J., Wyman, J., & Changeux, J. P. (1965). On the Nature of Allosteric Transitions: A Plausible
520 Model. *Journal of Molecular Biology*, *12*, 88–118. https://doi.org/10.1016/S0022-
521 2836(65)80285-6
522 Ohlendorf, R., Vidavski, R. R., Eldar, A., Moffat, K., & Möglich, A. (2012). From dusk till dawn: one-
523 plasmid systems for light-regulated gene expression. *Journal of Molecular Biology*, *416*(4),
524 534–542. https://doi.org/10.1016/j.jmb.2012.01.001

525 Olson, E. J., Hartsough, L. A., Landry, B. P., Shroff, R., & Tabor, J. J. (2014). Characterizing bacterial
526 gene circuit dynamics with optically programmed gene expression signals. *Nature Methods*,
527 *11*(4), 449–455. https://doi.org/10.1038/nmeth.2884
528 Pilizota, T., & Yang, Y.-T. (2018). "Do It Yourself" Microbial Cultivation Techniques for Synthetic and
529 Systems Biology: Cheap, Fun, and Flexible. *Frontiers in Microbiology*, *9*.
530 https://doi.org/10.3389/fmicb.2018.01666
531 Pudasaini, A., El-Arab, K. K., & Zoltowski, B. D. (2015). LOV-based optogenetic devices: light-driven
532 modules to impart photoregulated control of cellular signaling. *Frontiers in Molecular*
533 *Biosciences*, *2*, 18. https://doi.org/10.3389/fmolb.2015.00018
534 Raffelberg, S., Wang, L., Gao, S., Losi, A., Gärtner, W., & Nagel, G. (2013). A LOV-domain-mediated
535 blue-light-activated adenylate (adenylyl) cyclase from the cyanobacterium Microcoleus
536 chthonoplastes PCC 7420. *Biochemical Journal*, *455*(3), 359–365.
537 https://doi.org/10.1042/BJ20130637
538 Reimers, A.-M., Knoop, H., Bockmayr, A., & Steuer, R. (2017). Cellular trade-offs and optimal
539 resource allocation during cyanobacterial diurnal growth. *Proceedings of the National*
540 *Academy of Sciences of the United States of America*.
541 https://doi.org/10.1073/pnas.1617508114
542 Richter, F., Scheib, U. S., Mehlhorn, J., Schubert, R., Wietek, J., Gernetzki, O., … Möglich, A. (2015).
543 Upgrading a microplate reader for photobiology and all-optical experiments. *Photochemical*
544 *& Photobiological Sciences*, *14*(2), 270–279. https://doi.org/10.1039/c4pp00361f
545 Rockwell, N. C., & Lagarias, J. C. (2010). A brief history of phytochromes. *Chemphyschem*, *11*(6),
546 1172–1180. https://doi.org/10.1002/cphc.200900894
547 Romero, N. A., & Nicewicz, D. A. (2016). Organic Photoredox Catalysis. *Chemical Reviews*, *116*(17),
548 10075–10166. https://doi.org/10.1021/acs.chemrev.6b00057
549 Ryu, M.-H., Kang, I.-H., Nelson, M. D., Jensen, T. M., Lyuksyutova, A. I., Siltberg-Liberles, J., …
550 Gomelsky, M. (2014). Engineering adenylate cyclases regulated by near-infrared window
551 light. *Proceedings of the National Academy of Sciences of the United States of America*,
552 *111*(28), 10167–10172. https://doi.org/10.1073/pnas.1324301111
553 Ryu, M.-H., Moskvin, O. V., Siltberg-Liberles, J., & Gomelsky, M. (2010). Natural and engineered
554 photoactivated nucleotidyl cyclases for optogenetic applications. *Journal of Biological*
555 *Chemistry*, *285*(53), 41501–41508. https://doi.org/10.1074/jbc.M110.177600
556 Salomon, M., Eisenreich, W., Dürr, H., Schleicher, E., Knieb, E., Massey, V., … Richter, G. (2001). An
557 optomechanical transducer in the blue light receptor phototropin from Avena sativa.

558 *Proceedings of the National Academy of Sciences*, *98*(22), 12357–12361.
559 https://doi.org/10.1073/pnas.221455298
560 Schröder-Lang, S., Schwärzel, M., Seifert, R., Strünker, T., Kateriya, S., Looser, J., … Nagel, G. (2007).
561 Fast manipulation of cellular cAMP level by light in vivo. *Nature Methods*, *4*(1), 39–42.
562 https://doi.org/10.1038/nmeth975
563 Sorigué, D., Légeret, B., Cuiné, S., Blangy, S., Moulin, S., Billon, E., … Beisson, F. (2017). An algal
564 photoenzyme converts fatty acids to hydrocarbons. *Science*, *357*(6354), 903–907.
565 https://doi.org/10.1126/science.aan6349
566 Stierl, M., Stumpf, P., Udwari, D., Gueta, R., Hagedorn, R., Losi, A., … Hegemann, P. (2011). Light-
567 modulation of cellular cAMP by a small bacterial photoactivated adenylyl cyclase, bPAC, of
568 the soil bacterium beggiatoa. *Journal of Biological Chemistry*, *286*(2), 1181–1188.
569 https://doi.org/10.1074/jbc.M110.185496
570 Strack, R. L., Strongin, D. E., Bhattacharyya, D., Tao, W., Berman, A., Broxmeyer, H. E., … Glick, B. S.
571 (2008). A noncytotoxic DsRed variant for whole-cell labeling. *Nature Methods*, *5*(11), 955–
572 957. https://doi.org/10.1038/nmeth.1264
573 Stüven, B., Stabel, R., Ohlendorf, R., Beck, J., Schubert, R., & Möglich, A. (2019). Characterization
574 and engineering of photoactivated adenylyl cyclases. *Biological Chemistry*, *0*(0).
575 https://doi.org/10.1515/hsz-2018-0375
576 Szymula, K. P., Magaraci, M. S., Patterson, M., Clark, A., Mannickarottu, S. G., & Chow, B. Y. (2018).
577 An Open-Source Plate Reader. *Biochemistry*. https://doi.org/10.1021/acs.biochem.8b00952
578 Taslimi, A., Vrana, J. D., Chen, D., Borinskaya, S., Mayer, B. J., Kennedy, M. J., & Tucker, C. L. (2014).
579 An optimized optogenetic clustering tool for probing protein interaction and function.
580 *Nature Communications*, *5*, 4925. https://doi.org/10.1038/ncomms5925
581 Weissleder, R. (2001). A clearer vision for *in vivo* imaging. *Nature Biotechnology*, *19*, 316–317.
582 https://doi.org/10.1038/86684
583 Yee, E. F., Diensthuber, R. P., Vaidya, A. T., Borbat, P. P., Engelhard, C., Freed, J. H., … Crane, B. R.
584 (2015). Signal transduction in light-oxygen-voltage receptors lacking the adduct-forming
585 cysteine residue. *Nature Communications*, *6*, 10079. https://doi.org/10.1038/ncomms10079
586 Ziegler, T., & Möglich, A. (2015). Photoreceptor engineering. *Frontiers in Molecular Biosciences*, *2*,
587 30. https://doi.org/10.3389/fmolb.2015.00030

588 Figure Legends

589 ## Figure 1

590 The response of light-sensitive systems to pulsed illumination. **A**, In the simplest scenario, light 591 drives the transition of a monomeric photoreceptor from its dark-adapted state (D) to its light-592 adapted signaling state (L) with a unimolecular rate constant k_1 that depends on illumination 593 intensity. Once in the signaling state, the receptor thermally reverts to state D with a unimolecular 594 rate constant k_{-1}. In a somewhat more complex scenario, the photoreceptor be dimeric and capable 595 of populating an intermediate state with one protomer in the D, and the other in the L state. For 596 simplicity, the protomers are assumed to transition between the two photochemical states D and L 597 independently of another with the rate constants k_1 and k_{-1}, respectively. **B**, The kinetic scheme for 598 the monomer scenario was numerically solved in time for the indicated regime of periodic 599 illumination. Blue bars mark periods where light is applied and the D→L transition is hence 600 promoted; at other times, light is off, and the monoexponential L→D reversion predominates. The 601 ordinate denotes the fraction of the receptor in the L state. Two simulations for slow and fast dark 602 recovery with rate constants k_{-1} = 0.01 s^{-1} and 10·k_{-1} are shown as red and black lines, respectively. 603 Compared to the left panel, in the righthand one the frequency of pulsing is increased 4-fold and 604 the duration of each light period reduced by the same factor, thus retaining the same overall light 605 dose. **C**, The two panels report corresponding simulations for the dimer scenario, where the 606 ordinate shows the sum of the species DL, LD and LL. In contrast to panel B, the recovery reaction is 607 of sigmoidal functionality.

608 ## Figure 2

609 Schematic illustrating the application of programmable lighting in microtiter-plate (MTP) format. 610 A graphical user interface, implemented in Python/Qt, facilitates the configuration of the 611 programmable array of 64 light-emitting diodes (LED). The configuration file is uploaded to an 612 Arduino circuit board which controls the timing and intensity of the single LEDs in the array. The 613 array is encased in a 3D-printed housing and an MTP mounted on top to allow illumination of 614 individual wells from below (Hennemann et al., 2018; Stüven et al., 2019).

615 ## Figure 3

616 Optogenetic control of the pDusk system by pulsed blue light. **A**, The pDusk-*Ds*Red plasmid wires 617 the blue-light-inhibited two-component system YF1/*Bj*FixJ to the expression of the red-fluorescent 618 reporter *Ds*Red (Möglich et al., 2009; Ohlendorf et al., 2012). **B**, *Escherichia coli* bacteria harboring 619 pDusk-*Ds*Red were cultivated under different lighting regimes as controlled by the programmable 620 LED array. In periodic manner, illumination for 30 s at different intensities (denoted on the ordinate)

621 was followed by dark intervals of variable duration (abscissa). For each parameter setting, the
622 reporter fluorescence of three replicate bacterial cultures was averaged and is plotted as color code.
623 Data for the original pDusk system (left) are juxtaposed to data for a derivative pDusk system (right)
624 which employs the V28I variant of YF1 that features much decelerated recovery kinetics and is hence
625 effectively more light-sensitive (Hennemann et al., 2018).

626 ## Figure 4

627 Characterization of the red-light-responsive adenylyl cyclase *Dd*PAC (Stüven et al., 2019). **A**, The
628 pCyclR test bed for photoactivated adenylyl cyclases (PAC) relies on the inducible expression of PACs
629 in *Escherichia coli*. Upon stimulation with light, PACs ramp up the production of the second
630 messenger 3’, 5’ cyclic adenosine monophosphate (cAMP) which associates with the endogenous
631 catabolite activator protein (CAP) to enable upregulation of the expression of a *Ds*Red reporter
632 gene. **B**, Using the pCyclR system and programmable lighting, we probed the response of *Dd*PAC to
633 constant illumination of varying intensity and wavelengths of 655 (circles) and 850 nm (triangles),
634 respectively. *E. coli* cultures harboring pCyclR and *Dd*PAC were grown at the different light settings,
635 and *Ds*Red fluorescence of four biological replicates ± standard deviation is reported. **C**, As in panel
636 B, but cultures were intermittently illuminated with 655-nm light at 40 µW cm^{-2}. The abscissa
637 denotes the fraction of time for which light was applied.

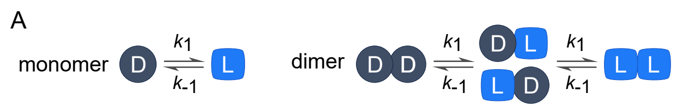
A
monomer
D
k_1
k_{-1}
L
dimer
D D
k_1
k_{-1}
D L
L D
k_1
k_{-1}
L L

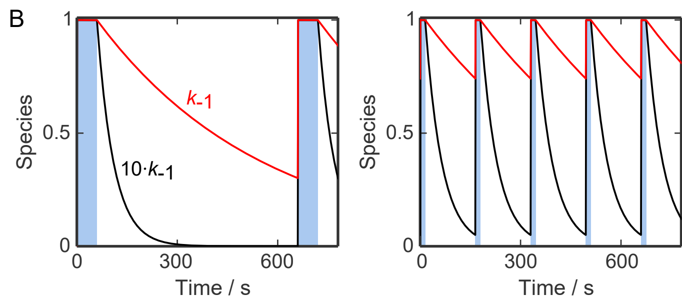
B
Species
Time / s
k_{-1}
$10 \cdot k_{-1}$
0
0.5
1
0
300
600

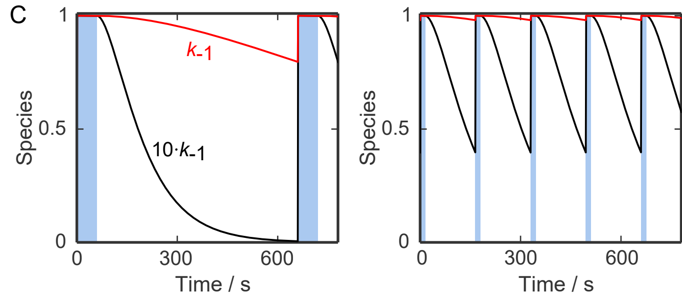
C
Species
Time / s
k_{-1}
$10 \cdot k_{-1}$
0
0.5
1
0
300
600

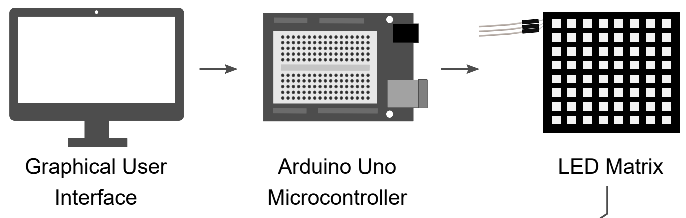
Graphical User Interface
Arduino Uno Microcontroller
LED Matrix

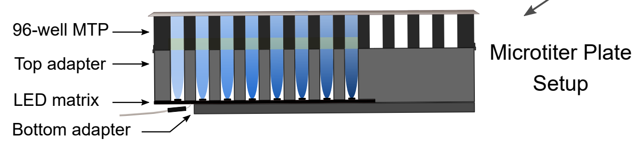
96-well MTP
Top adapter
LED matrix
Bottom adapter
Microtiter Plate Setup

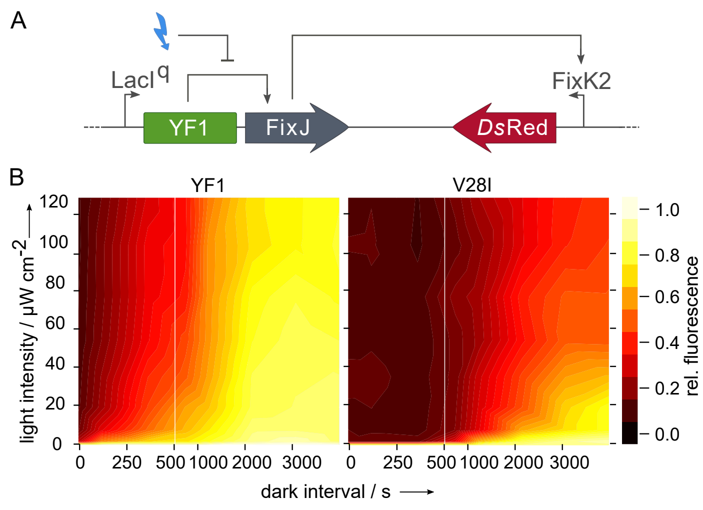
A
LacI q
FixJ
YF1
FixK2
DsRed
B
YF1
V28I
light intensity / µW cm-2
dark interval / s
rel. fluorescence
120
100
80
60
40
20
0
0
250
500
1000
2000
3000
1.0
0.8
0.6
0.4
0.2
0.0

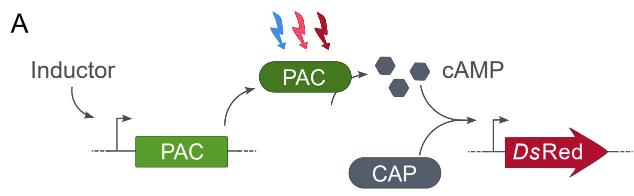
A
Inductor
PAC
PAC
cAMP
CAP
DsRed

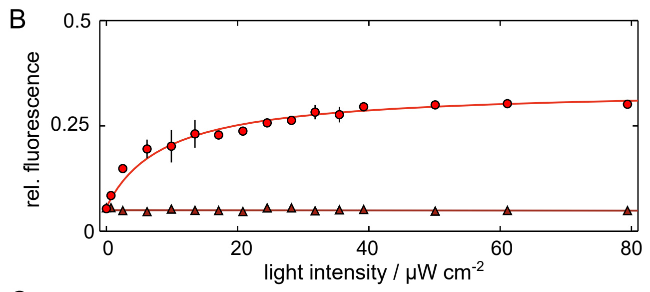
B
0.5
0.25
0
rel. fluorescence
0
20
40
60
80
light intensity / µW cm-2

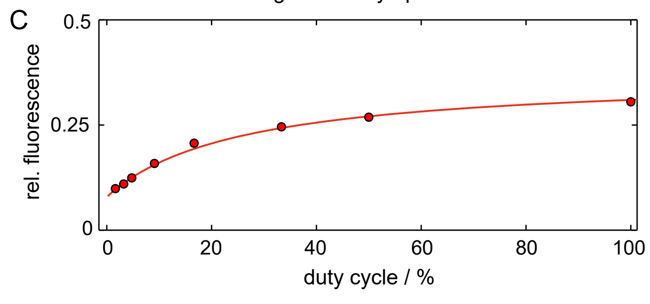
C
0.5
0.25
0
rel. fluorescence
0
20
40
60
80
100
duty cycle / %